Speed-up drivers for H 2 -enriched flames in Porous Media Burners

Enrique Flores-Montoya, Pierre-Alexandre Masset, Thierry Schuller, Laurent Selle

Speed-up drivers for H_2-enriched flames in Porous Media Burners

Enrique Flores-Montoya[a,*], Pierre-Alexandre Masset[b], Thierry Schuller[a,c], Laurent Selle[a]

[a] *Institut de Mécanique des Fluides de Toulouse, IMFT, Université de Toulouse, CNRS, Toulouse, France*
[b] *Université Paris-Saclay, CEA, Service de Thermo-hydraulique et de Mécanique des Fluides, Gif-sur-Yvette, 91191 , France*
[c] *Institut Universitaire de France (IUF)*

Abstract

An experimental study on the influence of porosity and hydrogen enrichment on the stabilization of premixed CH_4-Air flames in Porous Media Burners (PMBs) is presented. Flame stabilization is analyzed via direct flame front tracking, which is made possible by a novel experimental apparatus. The use of additive manufacturing for computer-generated topologies allows making optically-accessible PMBs featuring see-through directions. This methodology also enables topology tailoring which is here exploited to study the influence of porosity on burner's performance. Flame front tracking reveals a different stabilization trend in highly H_2-enriched flames. A comparison with a theoretical model is used to remove the effect of preheating and focus on other fuel properties. This suggests a flame-speed enhancement mechanism driven by Lewis number effects in $\mathrm{Le} < 1$ mixtures. Together with recent 3D Direct Numerical Simulations, these results provide evidence that preferential diffusion effects are key in the stabilization of flames in PMBs. These phenomena, not considered in state-of-the art 1D-Volume Averaged Models, remain crucial for the design of efficient PMB using hydrogen as a fuel.

Keywords: Flame Front Tracking; Additive Manufacturing; Hydrogen; Optical Access; Stabilization Mechanisms

Information for Colloquium Chairs and Cochairs, Editors, and Reviewers

1) Novelty and Significance Statement

The novelty of this research is the development of a pioneering experimental setup that provides direct flame front visualization in Porous Media Burners (PMBs). As a result, the flame front can be tracked, enabling a detailed analysis of flame stabilization mechanisms in CH_4-Air and H_2-enriched flames.
It is significant because it reveals the existence of stabilization mechanisms in H_2-enriched flames that are essentially different from those of CH_4-Air flames and are not taken into account in current models for combustion in inert porous media. An appropriate characterization of H_2 flames in PMBs will require the incorporation of these mechanisms.

2) Author Contributions

- E. F. M. Investigation, Software, Data curation, Visualization, Formal analysis, Writing - Original Draft
- P. A. M. Conceptualization, Formal analysis, Writing - Review & Editing
- T. S. Conceptualization, Formal analysis, Writing - Review & Editing, Supervision, Funding acquisition
- L. S. Conceptualization, Formal analysis, Writing - Review & Editing, Supervision, Funding acquisition

3) Authors' Preference and Justification for Mode of Presentation at the Symposium

The authors prefer **PPP** presentation at the Symposium, for the following reasons:

- Novel experimental setup: optically-accessible PMBs with see-through directions benefit visually from a poster's physical form.
- Complex background information: the paper relies on significant background information and requires a broader contextualization (experimental setup, theoretical model...).
- One-to-one level discussion will help the understanding and arise enriching discussions.

1. Introduction

The storage of excess renewable energy in the form of hydrogen is a viable path for the reduction of CO_2 emissions. The subsequent use of H_2 as a fuel requires addressing specific challenges such as flame stabilization and NO_x mitigation. In the present work, heat-recirculating burners are considered for their ability to address these issues. In such burners, energy from the burnt gases is transported towards the fresh reactants to preheat them. Thanks to preheating, flame stabilization is enhanced and ultra-lean combustion is attainable. This enables low flame temperatures thus abating NO_x emissions. Porous Media Burners (PMB) are heat-recirculating devices where a flame is stabilized within the cavities of a porous matrix. Owing to their outstanding properties [**?**], PMBs are well suited to achieve a low-NO_x carbon-free flame via lean hydrogen combustion. Surprisingly, few works have addressed the combustion of pure hydrogen-air in PMBs [**?** **?**]. Other studies have considered the effects of hydrogen enrichment on canonical fuels such as methane and natural gas [**?** **?**] and on alternative energy vectors such as ammonia [**?** **?**]. Hydrogen addition was found to have a remarkable impact on burner operation, shifting the stability map towards lower equivalence ratios [**?**]. The aforementioned studies focus on the evolution of the burner operating range and report changes in the temperature profiles and in pollutants emissions. However, they do not specifically address the stabilization mechanisms of these flames and how they are affected by hydrogen blending. Recent DNS have shown that preferential diffusion effects play a key role in the stabilization of H_2 flames in PMBs [**?** **?**]. This effect is not specifically taken into account in 1D models such as those used for PMBs [**?**].

Despite the intrinsic complexities associated to H_2, even with conventional fuels the modeling of porous media combustion is challenging [**?**]. So far, the use of opaque reticulated foams in experimental studies has hindered direct optical access to the interior of the porous matrix. Recently, [**?**] achieved a 3D reconstruction of the temperature field in both phases of a PMB by combining X-ray μCT and infrared thermometry. In [**?**], $CH^\star$ chemiluminiscence was used to study the local structure of CH_4-Air flames stabilized in a two dimensional array of cylinders with a staggered configuration. Despite these and previous remarkable works [**?** **?** **?**], the use of non-intrusive techniques and laser diagnostics in the literature is scarce. Moreover, the geometrical parameters of the porous structure are known to have a direct impact on the combustion properties [**?** **?**]. However, the influence of the matrix porosity, ϵ, is rarely assessed in experimental studies. Generally, variations of ϵ are small and in most cases are a side effect of the utilization of different foams rather than a controlled parameter. Recently, several works have considered computer defined geometries built via Additive Manufacturing (AM) [**?** **?** **?**]. This methodology allows for topology tailoring and has been applied to enhance the burner operating range via spatial gradation of the topological parameters [**?**]. Here, this approach is used to produce PMBs with see-through directions. As a result, optical access to the interior of the matrix is granted and direct probing of the flame front is enabled. Computer designed geometries allow the independent variation of pore size, d_p and void fraction, ϵ. Here, we address the influence of porosity on the burner performance by comparing two PMBs with the same pore size and different porosities, $\epsilon = 0.5$ and $\epsilon = 0.8$. The influence of hydrogen enrichment on the burner operating domain and on flame stabilization is also analyzed. The tracking of the flame position as a function of the operating conditions allows us to compare the stabilization of CH_4-Air flames and H_2-enriched flames. For these flames, our results indicate stabilization mechanism other than heat recirculation, which are not accounted for in present 1D models.

2. Experimental setup & procedure

A sketch of the experimental setup is presented in Figure **??**. Hydrogen, methane and air mass flow rates, denoted by $\dot{m}_{H_2}$, $\dot{m}_{CH_4}$ and $\dot{m}_{Air}$, are adjusted using Bronkhorst ELFLOW and Vöetglin Redy smart mass flow controllers. Premixed reactants go through a convergent section and a sintered steel plate to homogenize the flow. To mitigate the thermal drift, a cooling circuit sets the wall temperature at the straight duct section to $T_w = 293$ K. During operation, the temperature of the sintered steel plate increases due to the radiative heat exchange with the PMB base. Consequently, the incoming flow is mildly preheated. Two K-type thermocouples with different bead sizes are used to measure the reactants' inlet temperature T_{in} right before they enter the porous matrix. Following [**?**], these two temperature measurements are combined to override the effect of radiation on the thermal balance of the thermocouple. After this correction, the uncertainty in the inlet temperature measurement is $\delta T_{in} \simeq 10$ K.[1] This value is later used to compute the one-dimensional laminar flame properties for each operating point. For optical access, the cylindrical porous matrix is placed inside a quartz tube with inner diameter $D = 50$ mm and supported by an internal quartz with a smaller diameter. The burner height is $L = 30$ mm and its width is adjusted to obtain a porous-to-quartz gap smaller than the pore size at room temperature. This enables assembling and prevent breakage by thermal expansion during operation. The x axis is oriented in the streamwise direction and the origin is at the burner inlet. Throughout this paper, this coordinate is often expressed in nondimensional form by normaliz-

[1] This value was obtained applying a standard procedure for uncertainty quantification: $\delta f(x_i) = (\sum(\partial_{x_i} f.\delta x_i)^2)^{1/2}$. We retained the contributions of the temperature measurements, the mass flow rate and the bead emissivity.

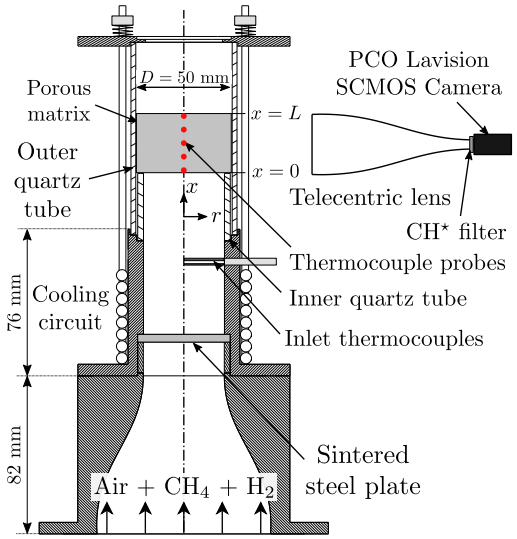

Fig. 1: Experimental setup.

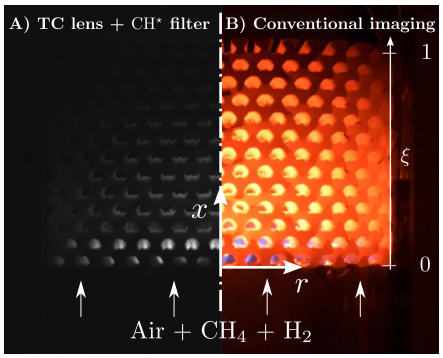

Fig. 2: CH* chemiluminiscence with TC lens (A) versus conventional imaging (B).

ing with the burner length, $\xi = x/L$. Additive Manufacturing (AM) is used to fabricate a PMB made of 316L stainless steel. This alloy exhibits a notable resistance to high temperature corrosion and its fusion temperature is about 1650 K. In our PMBs, the fluid-solid interphase is described by a Diamond-Triply Periodic Minimal Surface (Diamond-TPMS) defined by the implicit equation:

$$s(kx)s(ky)s(kz) + s(kx)c(ky)c(kz) + c(kx)s(ky)c(kz) + c(kx)c(ky)s(kz) = t \quad (1)$$

In Eq. (**??**), $s(\cdot)$ and $c(\cdot)$ stand for the sine and cosine functions while $k = 2\pi/\Lambda$ and t denote the lattice wavenumber and threshold respectively. These parameters, k and t, can be modulated to adjust the porosity, ϵ, and the pore size, d_p, of the structure. When computer-defined geometries are used, an exact representation of the topology is available through a CAD. Therefore, an accurate evaluation of the topological parameters of the burner can be performed thanks to several off-the-shelf tools such as PORESPY and OPENPNM. These parameters, including the solid and gas phase tortuosities, τ_s and τ_g, and the interphase volumetric surface, S_v, are gathered in Tab. **??**.

Table 1: Topological parameters of the PMBs.

d_p [mm]	ϵ	S_v [m^{-1}]	τ_g	τ_s
2.5	0.5	659	1.58	1.58
2.5	0.8	729	1.19	2.52

The resulting geometries offer various visual pathways in certain directions. These see-through directions provide optical access to the interior of the porous matrix and hence direct visualization of the flame front. In addition, they allow the insertion of thermocouples from the sides to measure the temperature in the burner. Temperature probes of type N with a sheath diameter of 0.5 mm are used to reconstruct the temperature profile along the symmetry axis of the burner. Inside the burner, thermocouples are subjected to a significant radiative flux from the solid matrix. This alters their thermal balance causing their temperature to lie somewhere between the solid and the gas temperature. A Lavision Imager SCMOS camera is aligned with one of the horizontal see-through directions of the porous matrix and used to visualize the flame. To maximize the signal intensity, the exposure time is set to 2000 ms. Due to perspective distortion, if a conventional optics is used, only the visual pathway aligned with the camera direction is completely cleared. To circumvent this issue, the camera is fitted with an Opto Engineering Telecentric lens TC4M-64. Telecentric (TC) lenses remove perspective distortion providing an orthogonal projection of the objects. Thanks to TC lens, we obtain a cleared optical access for all the visual pathways aligned with the exploration see-through direction. The image resolution is 2560×2160 px and with the TC optics the typical scale is about 23 μm per pixel. Because of the elevated temperatures reached during operation, the porous matrix radiates in the low visible range. To isolate the flame front region, the camera mounts an Edmund Optics bandpass filter with a central wavelength of 430 nm and a bandwidth of 10 nm. This allows collecting the line-of-sight integrated emission of the of the CH* radical. Figure **??** shows a comparison between flame visualization with a conventional imaging system and with the present optical setup.

The burner operating conditions are defined by the global equivalence ratio, ϕ, the load expressed in terms of thermal power, $P = \sum_f \dot{m}_f Q_f$, with $f = H_2$, CH_4, and the hydrogen power fraction, $\alpha_P = \dot{m}_{H_2} Q_{H_2}/P$. Here, Q_f denotes the fuel Lower Heating Value. The mean absolute uncertainty in the equivalence ratio is $\delta\phi = 0.008$ and the relative uncertainties in δP and $\delta\alpha_P$ are smaller than 3% and 4%, respectively. In this work, the focus is on

the submerged combustion regime, where the flame is stabilized inside the PMB and there is an intense coupling between combustion and heat transfer. However, submerged flames cannot be stabilized directly from cold start, a transient starting process is required to achieve this regime. The starting of PMBs is an overlooked topic in the literature. Generally, flames are first stabilized on top of the burner in the surface combustion regime. When multi-staged configurations are used, the transition from surface to submerged combustion is straightforward. Usually, ceramic foams with a small pore size are used for the upstream stages. This way, the upstream porous matrix acts as flame arrestor, quenching the flame and ensuring stability during the process. However, in single-staged configurations the transition from surface to submerged combustion is challenging. In CH_4-Air flames, the progressive reduction of the bulk to flame speed ratio often causes Flame Repetitive Extinction and Ignition (FREI) and is likely to result in flashback. Ceramic porous matrices feature a low resistance to thermal shocks [**?** **?**]. As a result, the burner operating conditions must be varied extremely slowly to prevent breakage. This imposes long transient times, further increasing the complexity of the starting process. Here, we propose a time-efficient method to achieve this transition that is made possible by the use of metallic burners. The procedure is detailed down below.

First, a CH_4-Air flame is stabilized on top of the burner in the surface combustion regime. Typically, the burner is started with a 0.8 kW CH_4-Air flame at $\phi = 0.6$. Then, to achieve submerged combustion conditions, a small fraction of hydrogen is temporarily added so as to pull the flame inside of the porous matrix. For $\epsilon = 0.8$ matrices, an increase of the hydrogen content to $\alpha_P = 20\ \%$ generally suffices to trigger the transition. The flame front is tracked live as it performs a *controlled flashback* across the porous matrix (see Fig. **??**). In the sequence of Fig. **??** snapshots are labeled with the elapsed time from the start of the transient phase. Note that a relatively fast transition can be achieved without matrix breakage. The enhanced thermal shock resistance has proven to be a major advantage of metallic PMBs when compared to their ceramic counterparts. Their improved durability largely simplifies burner operation by reducing the risk of fracture and hence the laboratory time. Continuous surveillance is needed during the transient phase in order to prevent a flashback once the flame is close to the inlet. When the flame reaches the bottom of the burner, hydrogen content, α_P, power, P, and equivalence ratio, ϕ are re-adjusted and set to a known stable operating point. The system is then allowed to reach thermal equilibrium.

The exploration of the burner operating range is performed by varying the mixture equivalence ratio, ϕ, at constant power, P, and hydrogen content, α_P. Close to flashback and blowoff limits, the equivalence ratio is varied in steps of $\Delta\phi = 0.01$. A step of equivalence ratio of $\Delta\phi = 0.02$ is used elsewhere. For

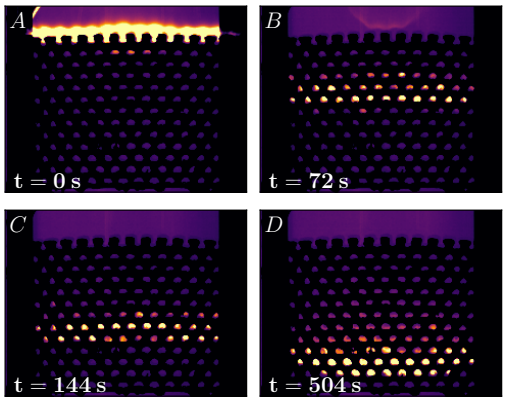

Fig. 3: *Controlled flashback* transient. (A) Ignition with CH_4-Air at $\phi = 0.6$. (B) Hydrogen addition to trigger transition to submerged combustion. (C) Removal of hydrogen. (D) Steady state in thermal equilibrium is reached.

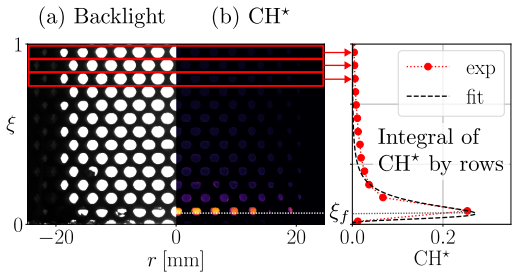

Fig. 4: Procedure to compute the axial profile of CH* and the flame position ξ_f.

CH_4-Air flames, the burner operation at high equivalence ratios was limited by overheating rather than by flashback. The thermal limit of the material is the major drawback of metallic PMBs. When the operating point of the burner is changed, temperature measurements are used to assess thermal equilibrium. Convergence is assumed when the maximum temperature variation over two minutes is less than 1 K for all thermocouples. For each experimental point, thermocouple and mass flow controller readings are recorded and averaged for two minutes. In parallel, an image of the flame inside the burner is taken. From images, the transversely averaged $CH^\star(x)$ profile is computed, which is assumed to be proportional to the heat release rate and it is used to compute the flame position inside the PMB. This allows tracking the flame as a function of the operating conditions. The procedure to compute the flame position from images is schematized in Fig. **??**. The images are first masked using a backlight mask. This also removes direct reflections in the solid matrix. The axial profile is obtained by computing the surface integral of $CH^\star$ intensity at each row of pores. The resolution of this raw profile is given by the spacing between the pores. It is equal to half the period of the lattice, $\Lambda/2$, and defines the uncertainty in the estimation of the flame

position, δx_f. The experimental profiles are then fitted by a beta-prime distribution for subgrid interpolation. The position of the flame, x_f, is taken as the location of the function maximum. For each operating point, the measured inlet temperature, T_{in} and the mixture composition defined by α_P and ϕ are used to compute the properties of the corresponding premixed laminar flame: the laminar burning velocity, S_{L_0}, the adiabatic flame temperature, T_{ad}, the flame thickness, $\delta_{T_0} = (T_{ad} - T_{in})/\max(\partial T/\partial x)$, the inlet gas density, ρ_{in}, and the Zeldovich number, Ze. More specifically, the Zeldovich number is computed as, $\mathrm{Ze} = E(T_{ad} - T_{in})/RT_{ad}^2$, where R is the universal gas constant and E is the activation energy, calculated from:

$$E = -2R\partial[\ln(\rho_{in} S_L)]/\partial(1/T_{ad}) \qquad (2)$$

The derivative in Eq. (**??**) is computed from two one-dimensional flames by performing small variations in the N_2 molar fraction while keeping the equivalence ratio and inlet temperature constant. This calculations are performed using CANTERA and the detailed kinetic scheme UCSD (57 species and 268 reactions) with mixture-averaged transport coefficients. Finally, temperatures are normalized as $\theta = (T - T_{in})/(T_{ad} - T_{in})$.

3. Results & Discussion

Figure **??** depicts three 1 kW CH_4–Air flames with distinct equivalence ratios stabilized in the $\epsilon = 0.8$ PMB. Post-treated images are presented in the left column, where the interpolated flame position is indicated with a white dotted line. On the right, the experimental profiles of $CH^\star$ and their beta-prime fit are displayed in red dotted and black dashed lines, respectively. Additionally, solid blue lines represent the normalized temperature profiles acquired via the thermocouples. Near the flashback limit, flames stabilize close to the burner inlet, as illustrated in the lower plot of Fig. **??**. As the equivalence ratio is decreased, flames gradually shift downstream, stabilizing at higher $\xi = x/L$ values. At the blowoff limit, top plot of Fig. **??**, flames stabilize approximately in the middle of the burner. Note that the flame front is reasonably flat across the transverse direction, which suggests that a one-dimensional model is a reasonable first approximation.

3.1. Influence of porosity

The influence of porosity on the PMB performance is now examined for CH_4-Air mixtures. Figure **??** shows the experimental points in the $P - \phi$ map for the two burners considered. The blowoff and high-temperature limits are marked with dashed and dash-dot lines, respectively. The shaded region outlines the estimated boundaries of the burner's operating domain. Dashed areas in the upper right corners denote unexplored regions due to thermal constraints of the material. In these zones, the elevated temperatures reached inside the PMB can lead to severe deformation of the porous structure. Figure **??** shows that the stability domain of the burner is directly affected by ϵ. When the porosity lowered from $\epsilon = 0.8$ to $\epsilon = 0.5$, the operating domain is shifted towards higher equivalence ratios. This can be explained by an analysis of the kinematic balance between the flow velocity, u_B, and the local flame speed, S_L. When the porosity is reduced, the effective burner section is reduced by the same factor and velocities inside the porous matrix increase for an imposed mass flow rate. Therefore, in order to ensure a kinematic balance between the flow and flame velocities, higher values of S_L are required. The local flame speed can be enhanced either by increasing the recirculation efficiency, η_{rec}, or by operating at larger equivalence ratios, ϕ. *Ceteris paribus*, recirculation efficiency decreases with porosity [**?**]. However, porosity variations also drive changes in other parameters such as the specific exchange surface, S_v, which directly scales the heat exchange term, h_v. Thus, predicting its influence is not straightforward in practice.

In PMBs, heat recirculation enables increasing the mass consumption rate per flame unit surface. This increase is quantified by the flame speed-up, defined as the ratio between the bulk velocity in the PMB, computed as $u_B = \dot{m}/(\rho_{in} A\epsilon)$, and the laminar burning velocity at inlet conditions, $S_{L_0}(\phi, T_{in})$.

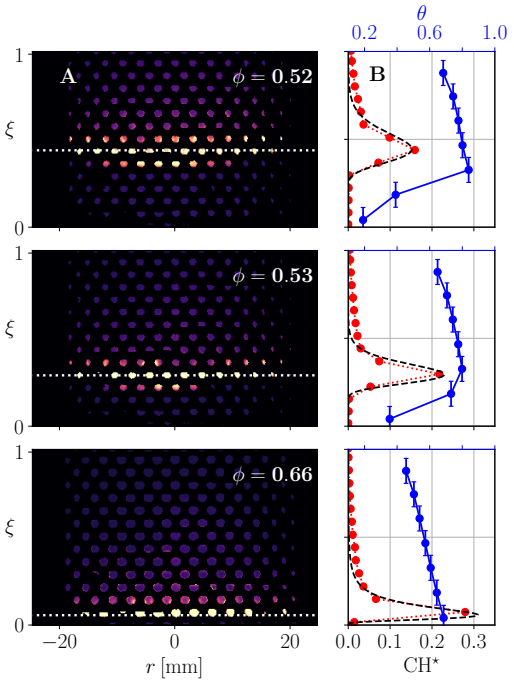

Fig. 5: A) Line-of-sight integrated $CH^\star$ signal for three 1 kW CH_4-Air flames at different equivalence ratios. B) Profiles of $CH^\star$ and normalized temperature, θ, as a function of the axial position, $\xi = x/L$.

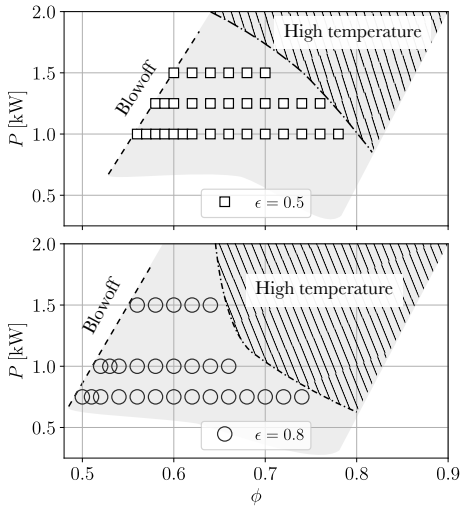

Fig. 6: Operating domain spanned by power, P, and equivalence ratio, ϕ, for CH_4-Air flames in PMBs with different porosities $\epsilon = 0.5$ and $\epsilon = 0.8$.

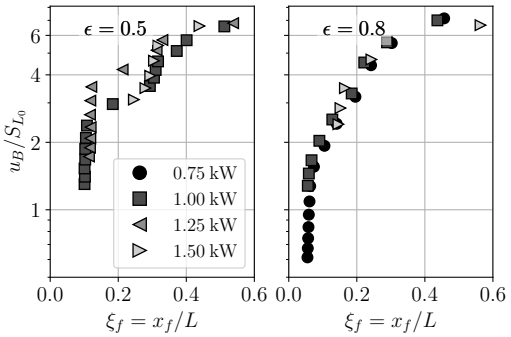

Fig. 7: Flame speed-up, u_B/S_{L_0}, versus flame position, $\xi_f = x_f/L$, at various powers for two porosities, ϵ.

Here, $\dot{m}$ and $A = \pi D^2/4$ denote the total mass flow rate and the burner section, respectively. In finite PMB, the speed-up is a function of the position of the flame in the burner [**?**]. Our novel experimental setup allows measuring the evolution of the speed-up with the flame position, x_f, and comparing it to theoretical predictions. Figure **??** displays the results for CH_4-Air flames with different powers for the two burners under investigation. For $u_B/S_{L_0} \simeq 1$, flames stabilize in the vicinity of the burner inlet, $\xi = 0$. Due to heat losses, some of these flames can feature a speed-up smaller than unity. Unfortunately, the overheating limit of the burner was here reached before flashback occurrence and thus the u_B/S_{L_0} at flashback is not available for CH_4-Air flames. When u_B/S_{L_0} is increased, the flame is progressively pushed towards the burner outlet. u_B/S_{L_0} is maximum around $\xi_f \simeq 0.5$ and a further increase in the bulk to laminar flame speed ratio leads to blowoff. At the blowoff limit, the flame speed-up rises to approximately $u_B/S_{L_0} \simeq 7$ in both burners. For the limited power range reported here, the burner load does not affect the flame stabilization in terms of $u_B/S_{L_0}(\xi_f)$. Overall, ϵ is found not to alter the speed-up at blowoff but it has an impact on the shape of the $u_B/S_{L_0}(\xi_f)$ curve. In periodic structures, local anchoring effects can result in discrete jumps of the flame front position. In the $\epsilon = 0.5$ PMB, the discretization of the flame position, ξ_f, is more relevant and results in a different shape of the speed-up stabilization curve. This explains the larger spreading of experimental points around $\xi_f \simeq 0.2$ in the $\epsilon = 0.5$ burner.

3.2. Influence of H_2*-enrichment*

The influence of hydrogen enrichment on flame stabilization is now discussed. The operating domain of the $\epsilon = 0.8$ burner spanned by Power, P, and equivalence ratio, ϕ is displayed in Fig **??**a. The blowoff, flashback and high temperature limits are indicated with dotted, solid and dashed lines, respectively. For the sake of clarity, no shadowed regions are included here. Different markers are used for each hydrogen power fraction, α_P. Note that the $\alpha_P = 0\%$ points in Fig. **??**a are those of Fig. **??** with $\epsilon = 0.8$. Empty markers denote operating points where the laminar burning velocity S_{L_0} is lower than $0.5\,\mathrm{cm\,s^{-1}}$. For those operating points, combustion in the absence of heat recirculation is virtually impossible. Safety considerations make of combustion beyond flammability limit a major asset of PMBs for practical applications. Hydrogen content has a first order impact on the operating equivalence ratios. As shown in Fig. **??**a, the operating domain of the burner is shifted towards lower equivalence ratios for increasing values of α_P. As a rule of the thumb, the operating equivalence ratio ϕ is reduced by $\Delta\phi = 0.1$ every time the hydrogen power fraction is doubled. In the $\epsilon = 0.5$ PMB (not shown here), operating domains are slightly shifted towards higher equivalence ratios but the overall behavior is the same. In Fig. **??**b, the speed-up u_B/S_{L_0} is plotted against the flame normalized position for different powers and hydrogen contents, α_P. The addition of hydrogen has a direct impact on the flame stabilization. A H_2-enrichment of $\alpha_p = 20\ \%$ results in an upward displacement of the stabilization curve, but the overall behavior remains roughly the same. A larger increase in the hydrogen content to $\alpha_P = 40\ \%$ drives a substantial change in the stabilization trend of the flame. For increasing u_B/S_{L_0} ratios, highly H_2-enriched flames remain attached to the burner inlet, anchoring to the first row of pores at roughly $\xi_f \simeq 0.05$. Then, when a critical speed-up is reached, these flames are blown off the burner. As the H_2 content is increased, the stabilization curve $u_B/S_{L_0}(\xi_f)$ becomes very stiff. This is a significantly different behavior than that usually predicted by Volume Averaged Models (VAMs) and theory and it was also observed in 3D DNS [**?**]. Note that the mass consumption rate per flame unit surface can rise to nearly $u_B/S_{L_0} \simeq 140$ for $\alpha_P = 80\ \%$. The $u_B/S_{L_0}(\xi_f)$ stabilization curves

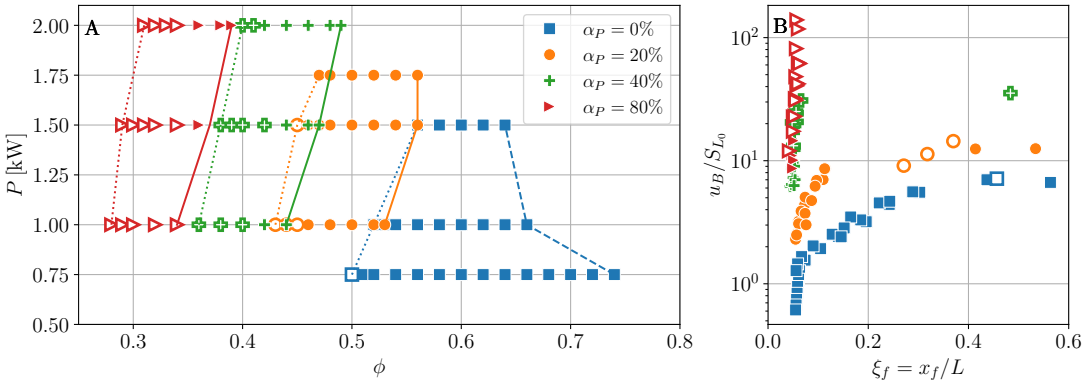

Fig. 8: A) Operating domain of the $\epsilon = 0.8$ burner for different hydrogen power fractions, α_P, in the $P - \phi$ space. B) Flame speed-up, u_b/S_{L_0}, versus normalized flame position, $\xi_f = x_f/L$, for different powers and hydrogen contents.

display a similar trend in the $\epsilon = 0.5$ burner.

Hydrogen flames feature larger Zeldovich numbers and are thus more sensitive to preheating than methane flames. However, in H_2-enriched flames, the different stabilization trends observed in Fig. **??**b suggest the existence of flame speed enhancement mechanisms other than preheating. To dig deeper into this question we compare the flame mass consumption rate observed in experiments, u_B, to the flame speed-up predicted by the asymptotic model of [**?**], S_{L_P}. In this theoretical model, heat recirculation is the sole flame-stabilization mechanism and mixture sensitiveness to preheating is accounted for via the Zeldovich number. Hence, variations in u_B/S_{L_P} with the hydrogen content hint towards the existence of other stabilization mechanisms. To compute S_{L_P} we impose the flame position observed in experiments, ξ_f and evaluate the theoretical model. Model parameters are computed as follows: topology dependent parameters are extracted from Tab. **??**; gas constants such as density, ρ_{in}, specific heat, c_{p_g}, thermal conductivity, λ_g, and viscosity, μ, are evaluated at the fresh gases temperature, T_{in}, and computed using the UCSD kinetic scheme; the interphase heat transfer coefficient is $h_v = S_v \lambda_g \mathrm{Nu}/d_p$, where the Nusselt number Nu is calculated using the correlation presented in [**?**] and the pore-based Reynolds and Prandtl numbers are defined as, $Re = \rho u_B d_p/\mu$ and $Pr = c_{p_g}\mu/\lambda_g$, respectively. A solid thermal conductivity of $\lambda_s = 13\ \mathrm{W\ m^{-1}\ K^{-1}}$ is assumed and radiative thermal losses at the burner ends are taken into account. In this asymptotic model [**?**], different expressions can be used to evaluate the flame speed ratio as a function of heat recirculation $S_{L_P}/S_{L_0}(\eta_{\mathrm{rec}})$. Here, the speed-up correlation developed by [**?**] is chosen.

Results are plotted in Fig. **??** as a function of the hydrogen molar fraction in the fuel, χ_{H_2}, for both burners. For each hydrogen content, u_B/S_{L_P} is averaged over the whole dataset and the vertical lines correspond to the maximum and minimum values. For CH_4-Air flames, the u_B/S_{L_P} ratio should be equal to one but the obtained values are about 0.7. This means that speed-ups measured in the experiment are smaller than those predicted by the asymptotic model. These differences can be attributed to the numerous simplifications made in the derivation of the asymptotic model. Strong assumptions such as constant transport coefficients and zero radial heat losses hinder quantitative predictions. However, these modeling limitations are expected to affect all flames rather equally, regardless of the fuel composition. Despite the fact that the model does not include radial heat losses, it does account for in/outlet losses by radiation. Switching them on/off only shifts the curves in Fig. **??** downwards by $2-7\%$ but does not affect the trends. Thus, comparing u_B/S_{L_P} ratios for different hydrogen contents the error should remain constant. In other words, if preheating is the sole mechanism responsible for flame speed-up, the u_B/S_{L_P} ratio should be independent of the mixture composition. Figure **??** reveals that the ratio between the observed and the predicted speed-up increases with the hydrogen molar fraction. Despite the significant dispersion in the results, the trend is clear and this supports the idea that a mechanism different from preheating affects flame speed-enhancement in H_2-enriched flames. Note that in Fig. **??**, the u_B/S_{L_P} ratio is also mildly affected by the porosity ϵ. This is because its influence on the speed-up is not quantitatively captured by the model. Changing the porosity affects other topological parameters that have a strong impact on h_v. Thus, the influence of porosity on simulations is, to a certain extent, encapsulated in h_v. The evaluation of the asymptotic model with different off-the-shelf correlations for the Nusselt number affects the predicted speed-ups yet it does not alter the conclusions drawn from Fig. **??**. For the sake of comparison, Fig. **??** shows the theoretical speed-up curves for 1kW CH_4-Air flames in the two burners with different porosity ϵ. The comparison between Figs. **??** and **??** confirms the overall qualitative agreement despite the over-prediction by the model. It has been checked that the kinetic mechanism is not at the ori-

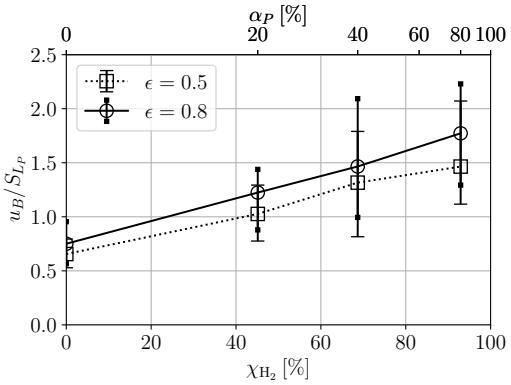

Fig. 9: Evolution of speed-up ratio with H_2 content.

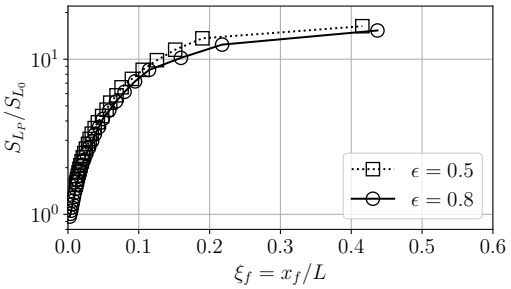

Fig. 10: Influence of ϵ on the burner speed-up in CH_4-Air flames.

gin of these discrepancies, which are very likely due to the underestimation of heat losses in the theoretical model.

For non-unity Lewis-number fuels such as H_2, preferential diffusion effects are known to play a major role in flame stabilization [**?**]. Recent 3D-DNS [**? ?**] revealed that the formation of locally enriched pockets caused by flame-front curvature has a strong impact on flame stabilization in PMBs. Therein, it was shown that hydrogen flames can accommodate larger mass flow rates by stretching and increasing their surface without moving downstream. Here, flame front tracking has revealed a different stabilization trend in highly H_2-enriched flames. Then, the influence of Zeldovich number has been removed via normalization by the theoretical flame speed S_{L_P}. Variations in the u_B/S_{L_p} ratio with hydrogen content suggest the existence of other flame speed enhancement mechanisms different from preheating in H_2-enriched flames. These results reinforce the claim that Lewis number effects must be taken into account for an accurate evaluation of the flame speed-up.

4. Conclusion

In this experimental study, direct flame visualization in a PMB has been achieved by means of an experimental setup where computer-generated topologies are built via additive manufacturing to produce optically accessible burners. Flame-front tracking has been used to study the influence of porosity and H_2-enrichment on flame stabilization in PMBs. The analyzed porosity variation was found to alter the operating equivalence ratios, ϕ, but did not affect the blow-off limit in terms of speed-up, $u_B/S_{L_0}(\xi_f)$. A comparison with the theoretical model presented in [**?**] reveals that quantifying the influence of porosity is challenging. This is because theoretical predictions are very sensitive to the modeling of the heat exchange term, h_v, which is in turn influenced by porosity variations. Moreover, H_2 enrichment is found to shift the operating domain towards lower equivalence ratios and to alter the flame stabilization. Qualitative differences between the stabilization of CH_4-Air and H_2-enriched flames suggest the existence of different stabilization mechanisms for non-unity Lewis-number fuels. Comparison with a theoretical model allows separating the sensitivity to preheating and brings to light other stabilization mechanisms. Variations of the u_B/S_{L_P} ratio with the hydrogen content point out the existence of other flame speed enhancement mechanisms in H_2-enriched flames. The present experimental results are consistent with recent observations made in 3D-DNS of premixed H_2-Air flames that could stabilize and accommodate large flow rates while being anchored at the inlet. Therein, preferential diffusion effects were shown to play a major role on flame stabilization in PMBs. The present experiments provide further evidence that these phenomena need to be modeled if an accurate description of the burning rate is sought. Future work must address these modeling tasks and seek pore-level diagnostics to unveil the details of flame stabilization in PMBs.

Declaration of competing interest

The authors declare that they have no known competing financial interests or personal relationships that could have appeared to influence the work reported in this paper.

Acknowledgments

The PhD of Enrique Flores Montoya is funded by BULANE and the Occitanie Region (*Défi Clé Hydrogène Vert*). Vincent Baylac (CIRIMAT) and Sebastien Cazin (IMFT) are acknowledged for their technical support with the manufacturing of the PMBs and with the optical diagnostics, respectively. The financial support of the European Research Council under the European Union's Horizon 2020 research and innovation program Grant Agreement 832248, SCIROCCO is also acknowledged.